

Nitrogen-rich mesoporous carbon for high temperature reversible CO₂ capture

M. Abdullah Khan^{a,*}, Ahad Hussain Javed^a, Memoona Qammar^a, Muhammad Hafeez^b, Muhammad Arshad^c, Mazhar Iqbal Zafar^a, Afrah M. Aldawsari^{d,e}, Afzal Shah^f, Zia ur Rehman^f, Naseem Iqbal^g

^a Renewable Energy Advancement Laboratory (REAL), Department of Environmental Sciences, Quaid-i-Azam University, Islamabad 45320, Pakistan

^b Department of Chemistry, University of Azad Jammu and Kashmir, Muzaffarabad, Pakistan

^c Nanoscience and Technology Division, National Center for Physics, Quaid-i-Azam University, Islamabad 45320, Pakistan

^d Chemistry Department, Faculty Applied Science, Umm Al Qura University, Makkah, Saudi Arabia

^e Petrochemical Research Institute, King Abdulaziz City for Science and Technology, P. O. Box 6086, Riyadh 11442, Saudi Arabia

^f Department of Chemistry, Quaid-i-Azam University, Islamabad 45320, Pakistan

^g US Pakistan Center for Advanced Studies in Energy, National University of Sciences and Technology, Sector H-12, Islamabad, 44000, Pakistan

ARTICLE INFO

Keywords:

Carbon capture
Mesoporous carbon

ABSTRACT

Selective CO₂ capture from a high temperature point source and its subsequent facile release is an important industrial challenge. It is well established that the nitrogen content can influence the CO₂ uptake selectivity of carbon-based adsorbent materials. This work presents an example of how nitrogen type and content in mesoporous carbon directly determines CO₂ uptake (and release) behaviour. Higher loadings of intrinsic nitrogen lead to increased isosteric heat of adsorption (Q_{st}) values, with selective low-pressure binding and large uptake of CO₂ at high temperature (75 °C). The process is reversible, only a mild vacuum exposure is sufficient to drive off the adsorbed CO₂, with sustained performance without a noticeable loss in activity. The work highlights the scope of the fine tuning the application specific structure of the adsorbent materials for optimal use.

1. Introduction

Carbon based fossil fuels are a vital source of energy. Their use in different sectors of the economy including power production, industries, transportation, production of a vast variety of chemicals, and pharmaceuticals is central to the current global economic growth [1,2]. However, the resulting CO₂ emissions from their continuous consumption are major contributors to the increasing levels of CO₂ in the atmosphere, the greenhouse effect, and consequent global warming [1,2]. This concern has prompted the need to develop materials and methods to capture these carbon emissions from thermal/coal-fired/natural gas-fired power plants to minimize their impact on the environment and for the sustainability of life on the planet [3–6].

In many industrial processes, CO₂ is present with other gases mainly N₂, and H₂O at low partial pressure and should ideally be recycled [7,8]. The conventional approach for post-combustion CO₂ capture is the use of aqueous solutions of alkanolamines [2,3,7,8]. In this process, CO₂ is

absorbed from a fuel gas stream into an aqueous solution of amines (20–30% concentration) at near ambient temperatures [6,9]. This occurs via chemisorptive formation of N–C bonded zwitterionic carbamate intermediates (chemical bonding enthalpies typically at ~ 100 kJ mol⁻¹) [5,6,10–12]. Setting aside the requirement of inhibitors for corrosion control, the high heat of absorption values of amines solution means, for the recovery of CO₂ from aqueous solution needs heating to high temperature (100–120 °C) with process steam. This is an inefficient method of CO₂ regeneration as it imposes an additional energy penalty and cost to the process [1,3,7]. The other methods include the use of solid porous materials for CO₂ capture, with several types of solid media reported to be effective [1,6,8,13–15]. However, the majority of porous carbons [8,16,17], zeolites [18], and metal-organic framework materials which are sensitive to the presence of water [5,19], etc. developed thus far demonstrate high uptake capacities only at low temperatures, where CO₂ is captured primarily through physisorption. Although the benefit of the physisorption process is low regeneration energy as compared to that

* Corresponding author at: Renewable Energy Advancement Laboratory (REAL), Department of Environmental Sciences, Quaid-i-Azam University, Islamabad, 45320, Pakistan.

E-mail address: makhan@qau.edu.pk (M.A. Khan).

<https://doi.org/10.1016/j.jcou.2020.101375>

Received 9 September 2020; Received in revised form 5 November 2020; Accepted 9 November 2020

Available online 28 November 2020

2212-9820/© 2020 Elsevier Ltd. All rights reserved.

required for amines, often it comes at the cost of sensitivity. That with a slight increase in temperature or moisture result in poor selectivity, thus deterring their employment for practical usage [5,20]. In a typical physisorption process, the heat of adsorption (an indirect measure of the binding strength of CO₂ to the material) for CO₂ capture employing these solid adsorbents is in the range of 15–30 kJ mol⁻¹, indicating a low energetic affinity for CO₂ adsorption [5,17,18]. Hence, the challenge lies in the design of a material with suitable heat of adsorption that enables the binding of CO₂ at high temperatures, together with minimal energy requirement for its release from the adsorbent. To date, the majority of adsorbent materials employed for CO₂ capture have emphasis is on the high CO₂ uptake where the aspect of tuning the CO₂ adsorption energy and requirement of low regeneration energy at a temperature relevant to real-world applications, is rather overlooked.

The other aspect of the problem in the post-combustion technique is low CO₂ capture efficiency when streaming a large volume gas at 40–60 °C in low pressure. A typical composition of the flue gas in power plants contains 15–16% CO₂ and 73–77% N₂ by volume, along with a small amount of water, SO₂, and O₂ [19,21]. Therefore the separation of CO₂ from N₂ is central to the post-combustion CO₂ capture. In general, research efforts to design adsorbent materials for CO₂ capture have two-fold focus. One is to enhance the CO₂ uptake capacity by (1) increasing surface area and modification of the pore networks [5,8,16,22,23] and/or (2) through the incorporation or grafting of basic groups into the adsorbent structure to optimize CO₂ uptake [13,22,24–27]. Since, the presence of amines at the surface/pores favor chemisorption over physisorption, the interaction phenomenon is complex [28–30]. It is generally assumed that acid-base interactions dominate the uptake process where (Lewis) basic nitrogen moieties capture (Lewis) acidic CO₂ molecules [3,31–35]. This has led to the investigations of many nitrogen-containing solids, supporting the role of Lewis basic sites for enhancing selective CO₂ capture [3,35–39]. However, a recent study has identified operative induction forces rather than acid-base interactions for improved CO₂ uptake behavior where negative electrostatic potentials serve as robust indicators for the effectiveness of N-doped sites to selectively capture CO₂ [22,29]. Further, the attempts have been devoted to synthesis materials containing nitrogen with different bonding environments that in turn show differences in energy enthalpies for the carbon capture process [13,32,34,40–42]. For instance, 2D and 3D mesoporous carbon structures having different pores, [42,43], and biomass-derived low temperature doping methods to produce nitrogen-doped mesoporous carbon were developed [17,36]. Similarly, porous carbons incorporated with N species have been reported to act as simultaneous CO₂-philic sites and pore-foaming agents

[44]. Despite this remarkable progress, the role of nitrogen content to the change in isosteric heat of adsorption values (Q_{st}) values and at high temperature CO₂ uptake in low pressure regime is relatively less explored. Therefore, a porous solid having intrinsic nitrogen embedded in the structure with moderate CO₂ heat of adsorption could be a good candidate for achieving easy on/easy off reversible CO₂ capture.

Here, we report the synthesis of high surface area nitrogen-rich mesoporous carbon materials and their corresponding CO₂ and N₂ uptake behaviors. The mesoporous carbon materials were prepared using a hard template method with varying ratio of EDA/CTC, diethylenetriamine/CTC, or triethylenetetramine/CTC to achieve high nitrogen content in resulting structures for efficient and selective carbon capture. The change in nitrogen (sp²/sp³-hybridized) content accompanied an increase in CO₂ uptake at high temperatures (75 °C), present isosteric heat of adsorption (Q_{st}) values higher than the physisorbed solids, yet lower than that of amines solutions, necessary for energy-efficient regeneration of adsorbents.

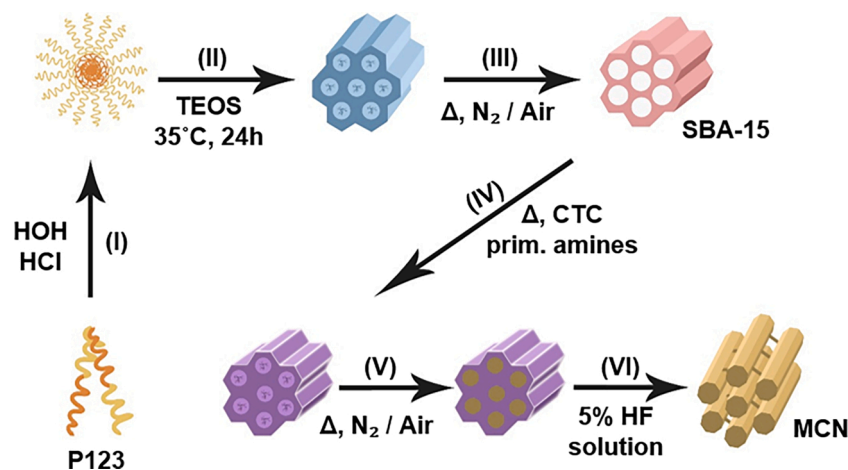
2. Experimental section

2.1. Synthesis of mesoporous silica

All the materials were used as supplied (Sigma-Aldrich) without further purification. Mesoporous silica (SBA-15) used in this work was synthesized according to the reported method using amphiphilic triblock copolymer, poly(ethylene glycol)-block-poly(propylene glycol)-block-poly(ethylene glycol) Pluronic P123, as a surface directing agent and tetraethyl orthosilicate (TEOS) as silica precursor (Scheme 1) [42]. In a typical synthesis, 4.0 g of Pluronic P123 was dissolved in 30 g of water and 120 g of 2 M HCl solution at 35 °C. Then 8.50 g of TEOS was added into that solution with stirring at 35 °C for 24 h. The mixture was then aged in static conditions at 100 °C. The obtained product was recovered, washed, and dried at room temperature which was subsequently calcined at 500 °C in a tube furnace with a heating rate of 5°/min in the air for 6 h.

2.2. Synthesis of nitrogen-rich mesoporous carbon (MCN)

To prepare MCN, an already published method with modification was followed [42]. The synthesized SBA-15 was used as a sacrificial template in the polymerization reaction between ethylenediamine (EDA) and carbon tetrachloride (CTC). The textural feature and porous structure of the carbon nitride (replica of the parent template) were maintained according to the silica template which in turn was



Scheme 1. Presentation of steps involved in the synthesis of silica template (SBA-15) and nitrogen rich mesoporous carbon (MCN) materials. The steps include; (I) micelle formation (II), self-assembly (II), thermal annealing (IV) precursor impregnation and polymerization (V) carbonization, and (VI) treatment with a 5% HF solution to remove silica template.

dependent on the chain length of the directing agents, reaction time, temperature, and concentration of the precursor (Scheme 1). Typically, 0.5 g of the prepared SBA-15 was added to the mixture of ethylenediamine (1.35 g) and carbon tetrachloride (3 g). The mixture was then refluxed and stirred at 90 °C for 6 h. The obtained dark brown solid was dried in an oven for 12 h and grounded to a fine powder. Afterward, the composite powder was carbonized under a nitrogen flow of 60 mL/min with a heating rate of 3.5°/min from room temperature to 600 °C and held there for 6 h. The product was then dissolved in a 5% HF solution for the removal of the silica template, followed by washing several times with ethanol and dried at 100 °C. A set of three samples with 1:1 EDA/CTC, (MCN1) Diethylenetriamine/CTC (MCN2), and triethylenetetramine/CTC (MCN3) were prepared. The experiments for higher amines ratios resulted in a sticky jelly-like mass that was not suitable for subsequent synthesis steps.

2.3. Characterization

Small angle X-ray diffractions patterns were measured on a Phillips

PW1729 diffractometer, operating in Bragg–Brentano focusing geometry and using Cu K α radiation ($k = 1.5418 \text{ \AA}$) from a generator operating at 40 kV and 30 mA. The diffractograms were recorded from 0.6° to 5°, with a step size of 0.01 and a step time of 1 s. SEM, images were recorded on JEOL 6500 F FEG SEM with a voltage of 5KV and a working distance of 10 mm. Transmission electron microscopy (TEM) images were recorded on JEOL 2010 equipped with a high-resolution pole piece running at 200 kV accelerating voltage. Samples were prepared by dispersing the powder products as of slurry in 1:1 water-ethanol solution which was then sonicated for 10 min before being deposited and dried on Agar Scientific 400 mesh Cu holey carbon support. The Fourier transform infrared (FTIR) was performed on a Nicolet 6700 FT-IR spectrometer with a MCT detector cooled using liquid nitrogen. The obtained spectra are averaging the 128 scans with a 4 cm^{-1} resolution. Elemental analysis was carried out using the Vario MICRO series CHNOS Elemental Analyzer. N₂ sorption was carried out using a Sorptomatic 1990 with CE Instruments analytical software. All the samples were outgassed at 473 K for 6 h before the N₂ adsorption measurements. N₂ gas adsorbate was used with 2 min equilibration times at each point and

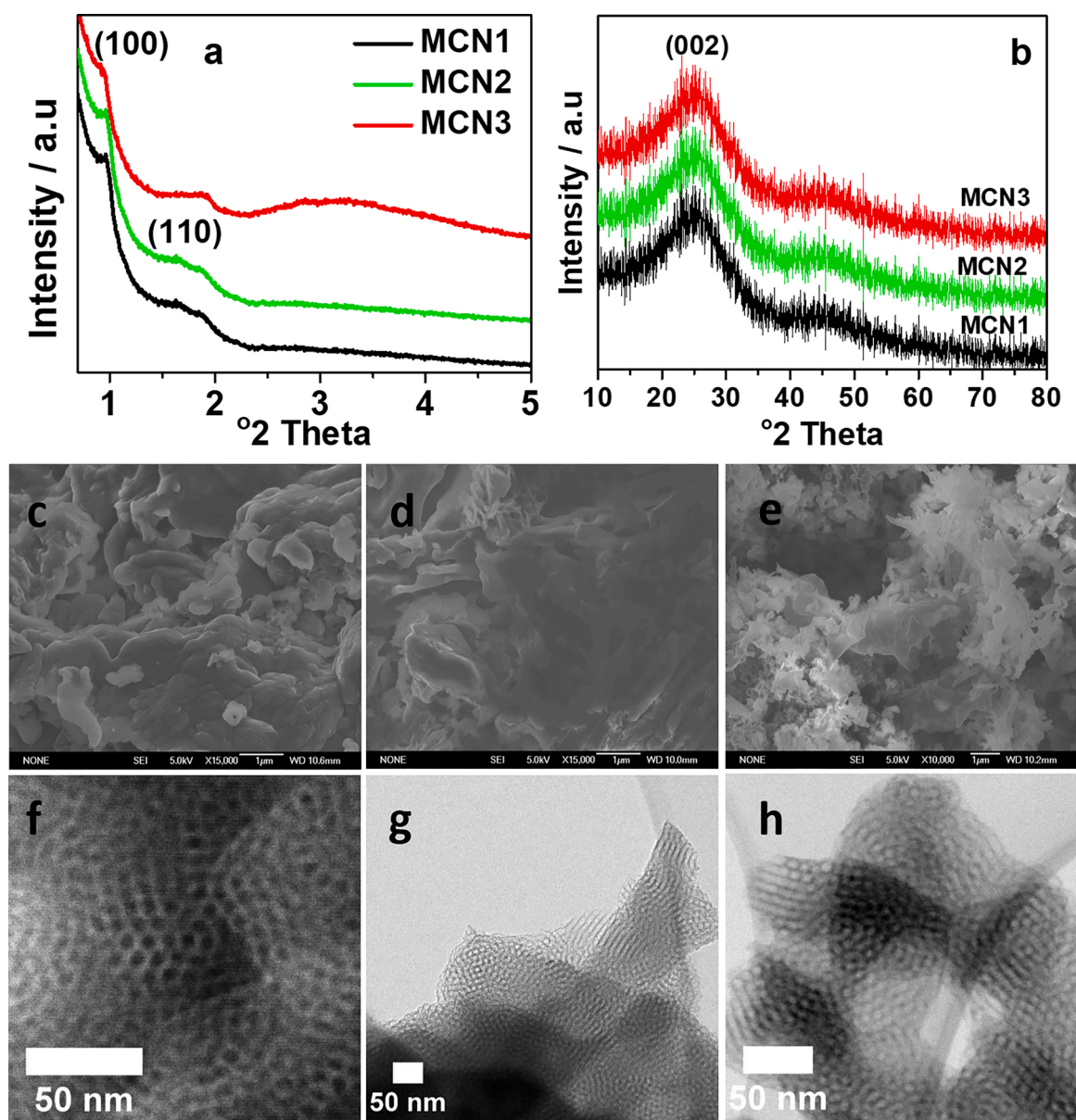


Fig. 1. The (a) small angle XRD (b) PXR of MCN materials. (c) SEM and TEM image of the MCN materials (c, f) MCN1, (d, g) MCN2, (e, h) MCN3 respectively.

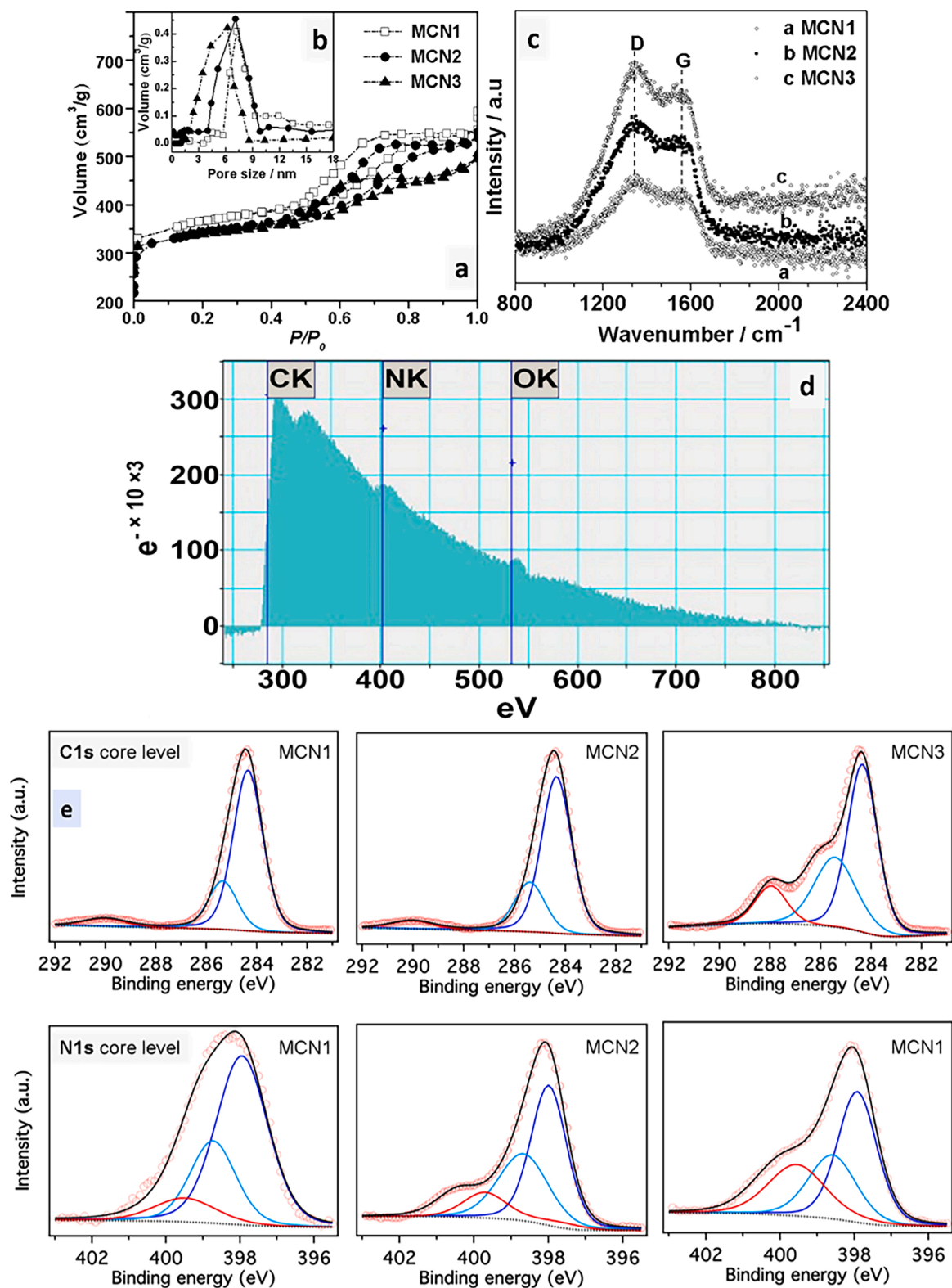


Fig. 2. (a) N₂ sorption isotherms of MCN (b) the inset shows the pore size distribution in MCN materials and (c) Raman spectra and (d) electron energy loss spectra of MCN3 (e) XPS C1s and N1s spectra of MCN materials.

a bath temperature of 77.2 K. The diameter volumetric distribution and mean pore diameter was determined by the Barrett–Joyner–Halenda (BJH) method, from the adsorption branch of isotherm, and the total pore volumes were estimated from the adsorbed amount at the constant C, where a relative pressure of $P/P_0 = 0.90$ was set. According to the accuracy of the instrument, the error is within 2%, so error bars are not

visible on the scales used. The X-ray photoelectron spectroscopy (XPS) measurements have been performed using a Scienta-Omicron system equipped with a micro-focused monochromatic Al K-alpha (1486.7 eV) and charge neutralizer CN10. The source was operated at 15 KeV with constant analyzer energy (CAE) 100 eV for survey scans and 20 eV for high-resolution scans. The data acquisition was done with Matrix

software and analysis was performed with Igor pro along with XPS fit procedures. The Curve fitting of high-resolution spectra was done by employing the Gaussian-Lorentzian (70–30%) line shape after performing the Shirley background corrections. The binding energy calibration was performed with C1 s core level at 284.8 eV.

2.4. Gas adsorption measurements

The CO₂ uptake isotherms were determined by using the Intelligent Gravimetric Analyser (IGA), model IGA-003, Hiden Analytical. The IGA-003 system has a software-controlled; thermostated microbalance with a weight resolution of 0.1 µg, and an ultra-high vacuum of (<10⁻¹ Pa). In a typical measurement, samples were degassed first at 423 K for 5 h to remove the physically adsorbed species/molecules. After the pretreatment system was kept under vacuum and temperature was adjusted to the value (25 °C or 75 °C) for measurement. The admittance of CO₂/N₂ to analyze actual adsorption equilibrium time at pressure points and the increase in the adsorbent weight was recorded automatically.

To calculate the enthalpies of adsorption for CO₂ on MCN materials Clausius- Clapeyron equation was employed at different temperatures (at 298, 308, 323, and 348 K). In each case, the data were fit using the equation:

$$(\ln P)_n = - (Q_{st}/R)(1/T) + C$$

where P is the pressure, n is the amount adsorbed, T is the temperature, R is the universal gas constant and C is a constant. The isosteric heat of adsorption Q_{st} was subsequently obtained from the slope of plots of $(\ln P)_n$ as a function of $1/T$, and the obtained values at the onset of adsorption are used for comparison [13,31,41]. The regeneration test was conducted using IGA, at room temperature and, 75 °C by exposing the material to a CO₂ atmosphere alternating between 6 mbar and 1 bar.

3. Results and discussions

The formation of the template replicated structure was confirmed with X-ray diffraction (XRD) analysis. Small angle X-ray diffraction patterns of synthesized samples are shown in Fig. 1a. The patterns exhibited retention of 2D hexagonal structure of the silica template in all mesoporous nitrogen-rich carbon (MCN) materials. Although, the position and intensity of the (100) peak is less intense and shifted to a lower angle in comparison to the parent template (Figure S1b), are remarkably clear, indicating the formation of interlinked mesostructures of pores interconnecting the walls. The weak intensities of the (110) and (200) reflections in MCN samples are likely due to the partial filling of the SBA-15 template, and the density contrast of silica walls to the MCN matrix [42,43]. In addition to the low angle 2θ values, powder XRD patterns (Fig. 1b) display a broad (002) diffraction peak at 26° of typical graphitic carbon structures having an interlayer d -spacing of 3.42 Å. Further, the surface morphology features of the materials examined through SEM present the existence of porous character (Fig. 1c–e), while the high-resolution transmission microscopy (HR-TEM) images show that the ordered mesopores in honeycomb arrangements are visible (Fig. 1f–h), and hexagonal mesostructure of silica template is preserved after its removal (Fig. S1a). The FTIR analysis of MCN materials showed bands corresponding to the symmetric and asymmetric stretching of primary amines (3204 and 3359 cm⁻¹) suggesting the presence of free amino groups (Fig. S3). The weak band of secondary amines in the same region is perturbed by the primary amines band. This reflects that nitrogen is present in the form of C–NH and C–NH–C, respectively. Other strong bands in the 1600–1150 cm⁻¹ region, attributed to the stretching mode of aromatic ring heterocycles or free N–H bending mode, and a broad band at 1226 cm⁻¹ assigned to vibrations of the C–N bond, are seen. These results infer the existence NH₂, N–H, or other N bonded basic groups in MCN structures.

To investigate the BET surface area, N₂ adsorption isotherms for

Table 1

Textural properties and N contents of nitrogen rich mesoporous carbon materials.

| Sample | S_{BET} m ² /g | D_{pore} (nm) | Chemical composition wt.% | | | C/N | I_D/I_G |
|--------|-----------------------------|-----------------|---------------------------|------|-----|------|-----------|
| | | | C | N | H | | |
| MCN1 | 540 | 7.4 | 72.8 | 19.5 | 4.9 | 3.73 | 1.01 |
| MCN2 | 526 | 6.9 | 67.4 | 21.9 | 4.8 | 2.92 | 1.04 |
| MCN3 | 514 | 6.1 | 66.8 | 26.1 | 4.7 | 2.56 | 1.09 |

MCN materials were performed (Fig. 2a). The resulting isotherms exhibit type IV behavior and are completely reversible. A slight decrease in the surface area (540, 526, 514 m²/g) and pore volume with increased nitrogen content was noted (Table 1) that can be attributed to the formation of a denser structure with increased nitrogen loadings. While in Raman spectra of MCN materials, both D and G bands in the range of 1334–1402 and 1554–1587 cm⁻¹, respectively are present (Fig. 2b). The G band in all samples is shifted to lower wavenumbers (1557 cm⁻¹) in comparison to the ordered graphitic carbon (1584 cm⁻¹) [45]. This shift towards lower wavenumbers, the appearance of D band, and the high ratio of I_D/I_G (1.01–1.09) in MCN materials indicated the presence of sp³ carbon/nitrogen species. It is important to note that the shift of G band to lower wavenumbers (from E_{2g} ideal graphitic phase) is highest in MCN3, which suggests the incorporation of N atoms into the structure along with the increased distortion of the graphitic phase.

The elemental analysis of the materials revealed the N content increases in MCN1 < MCN2 < MCN3 (Table 1). The electron energy loss (EELS) spectrum of MCN3 from the edge of a sample fragment is shown in (Fig. 2c). The spectrum has been deconvoluted with the zero-energy loss peak to give an approximation of single scattering signal, as the sample is generally too thick for single scattering featuring the sharp C and N K-edge peaks. Three observed peaks at 292 eV, 320 eV, and 403 eV can be ascribed to C and N K-edges and the small peak at 540 eV due to traces of the oxygen present as typical background, indicates that the sample is mainly composed of C and N. The sharp peak at 292 eV is evidence of transitions from 1 s core to π^* band and can be attributed to sp²-hybridized carbon bonded to nitrogen. Additionally, the broad band at 320 eV in the CK-edge spectrum is due to transitions from characteristic 1s- σ^* states indicating the sp² hybridization of carbon in all samples. The N K-edge peak at 403 eV is also evidence of the sp² hybridized N atoms and supports the conclusion drawn from the C K-edge peak analysis of the EEL spectrum. However, the relative broadness of the N K-edge peak is also indicating the presence of the sp³ hybridized N atoms [37,42].

The XPS C1 s and N1 s spectra of MCN materials are presented in Fig. 2e. The C1 s, spectra of MCN3 show three deconvoluted peaks at 284.56, 285.83, and 288.36 eV that can be assigned to pure graphitic carbon, carbon bonded to N, and sp² C attached to amines, respectively. In contrast, the C1 s spectra of MCN2 and MCN1, show two main peaks where 288.36 eV peak, which stems from sp²-hybridized C in aromatic rings attached to an electronegative –NH₂ or –NHR group, is greatly suppressed. While the peaks at 284.56 eV, which correspond to sp²-hybridized C atoms bonded to N inside the conjugated ring, are dominant. These results indicate the existence of a largely aromatic structure. The observed N1 s spectra of MCN materials show three peaks at 399.8 eV (C–NH₂), 398.7 eV (C–NH), and 398.0 eV (C–N). The appearance of these peaks mainly results from nitrogen participating in the different aromatic domains and as a terminal group. The peak at 399.8 eV is therefore assigned to N atoms bonded to two sp²–C atoms, while the peak at 398.7 eV can be attributed to the sum of N_{bridge} (N bonded to three sp²–C, –NH– bonds) and N_{terminal} (NH₂) groups. Notably, the area under the curve for peaks at higher binding energy in MCN3 is significantly greater. It can be concluded that the MCN3 structure is a mix of sp²-hybridized C network where N atoms are substituted in aromatic rings or connecting sp² microdomains along with the –NH₂ terminal groups which are consistent with the results reported previously [37,

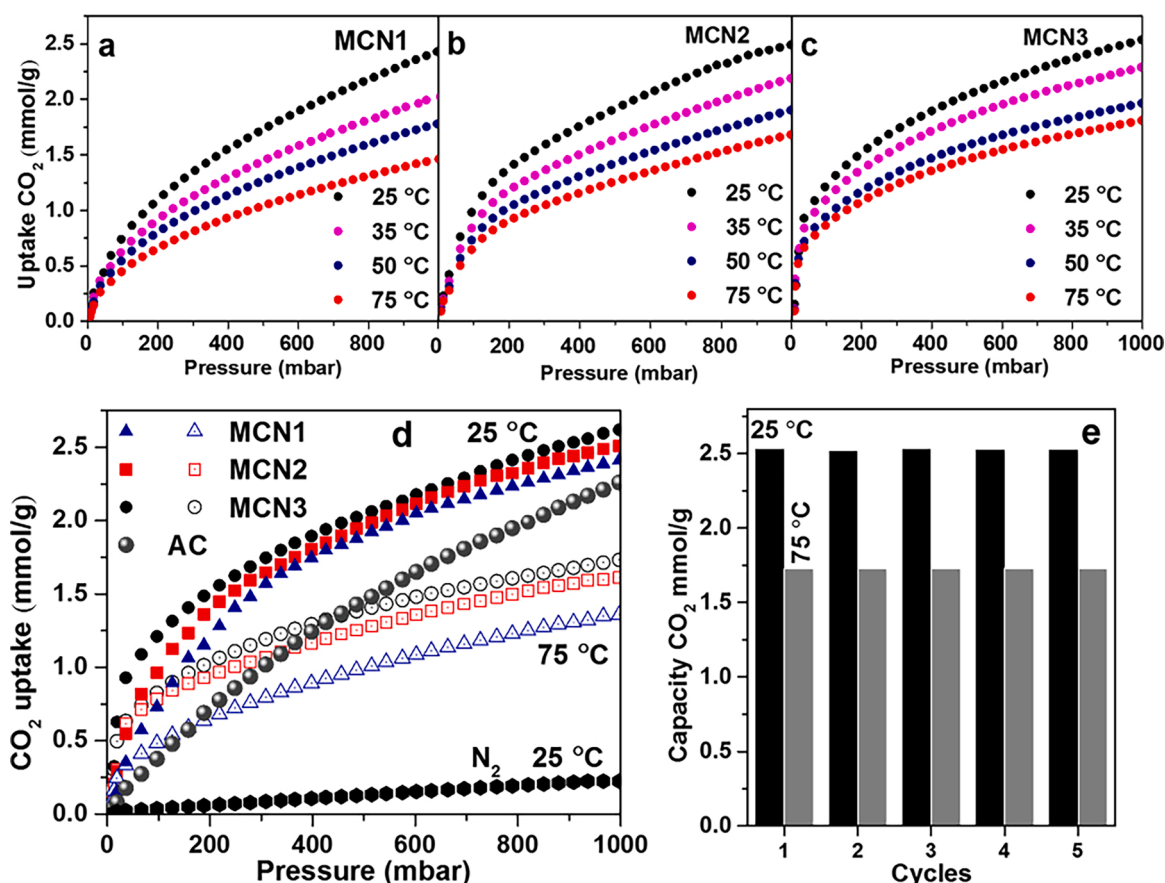


Fig. 3. (a–c) CO₂ sorption isotherm of MCN materials carried out at different temperatures (d) a comparison CO₂ uptake capacity of MCN materials and activated carbon, (e) cyclic tests of CO₂ adsorption on MCN3.

42]. It is noteworthy that the use of long-chain amine precursor for thermal condensation leads to increased N content in final structures, however, the aromatic character of the MCN3 has decreased. These subtle variations in chemical features make these structures extremely interesting for CO₂ uptake investigation.

The CO₂ uptake behavior of intrinsically nitrogen-rich carbon materials is compared in Fig. 3a–c. All of the samples show remarkably good and almost similar CO₂ uptake capacity (2.46–2.51 mmol/g) at 25 °C. In contrast, marked differences in CO₂ uptake capacity of materials were observed at 75 °C and 1 bar where MCN3, with highest N content, showed the largest uptake (1.74 mmol/g) followed by MCN2 (1.60 mmol/g), and MCN1 the lowest (1.24 mmol/g). This trend clearly shows that under these conditions higher nitrogen content is responsible for a high uptake of CO₂ at elevated temperatures and the result is consistent with earlier findings [35,38]. Also, the role of the BET surface area can be ruled out, as MCN1 has the highest surface area in comparison to the rest of the samples (Table 1). It is important to mention that activated carbon (AC) having surface area 574 m²/g, however, devoid of N content show almost similar CO₂ adsorption capacity (2.03 mmol/g) at 25 °C, but its uptake drastically dropped when measured at 75 °C (0.76 mmol/g). The other reported carbon based materials exhibit a similar trend for CO₂ uptake capacity at higher temperatures [13,39,46].

A comparison of CO₂ and N₂ adsorption isotherms for MCN and AC at 25 °C are presented in Fig. 3d. At low pressures (up to 20 mbar), particularly MCN3 exhibit higher CO₂ adsorption: 0.628 mmol/g versus 0.0824 mmol/g in AC. Besides, slight differences in adsorption behavior (line shape) exist till 500 mbar, but above 500 mbar, CO₂ adsorption of AC improved significantly (2.03 mmol at 1 bar) and becomes similar to MCN materials. A probable explanation for this behavior is the greater affinity of terminal amines towards CO₂, which triggers steep CO₂

uptake in low pressure regime suggesting chemisorption is operative here [35,47]. That follows the filling of pores at higher pressures. Note the intrinsic nature of amines and mesoporous pores (pore diameter 6.1–7.4 nm) of all MCN materials leaves terminal alkylamine sites exposed for interaction. For that reason after low pressure binding, CO₂ adsorption isotherms attained plateau rather quickly. Setting aside the stability concerns of previously studied carbon or carbon containing basic functionalities tethered at the surface/structures, their CO₂ uptake capacity at high temperature drop rapidly [5,35,47]. It is significant that metal free materials, made only with abundant C, H, and N elements show such high uptake at high temperature and low pressures. Furthermore, as the separation of CO₂ from N₂ is central to the post-combustion CO₂ capture process, when MCN3 was exposed to the N₂ gas it exhibited only ≈ 0.18 mmol/g uptake at 1 bar, a factor crucial for practical application.

The reversibility of CO₂ adsorption capacity of MCN3 at room temperature and 75 °C was assessed gravimetrically by exposing the material repeatedly to a CO₂ atmosphere alternating between 6 mbar (CO₂ removal) and 1 bar (CO₂ uptake) for five cycles. The results show that isotherms are completely reversible and uptake capacity in measured cycles remained almost unaltered, (Fig. 3e). For recovery, combined heat treatment and mild vacuum was applied. It was found that at 80 °C, 1 h, 95% CO₂ was driven off while at 100 °C, 1.5 h complete removal was noted. As the temperature of the flue-gas emitted from power plants is high, these results highlight the utility of MCN materials for low pressure post combustion capture. In addition, small angle XRD patterns and FTIR spectra of the spent MCN3 after adsorption-desorption cycles exhibit no change, infer that both pore network and chemical structure is intact after repetitive uptake cycles.

To understand the superior uptake and facile release of MCN

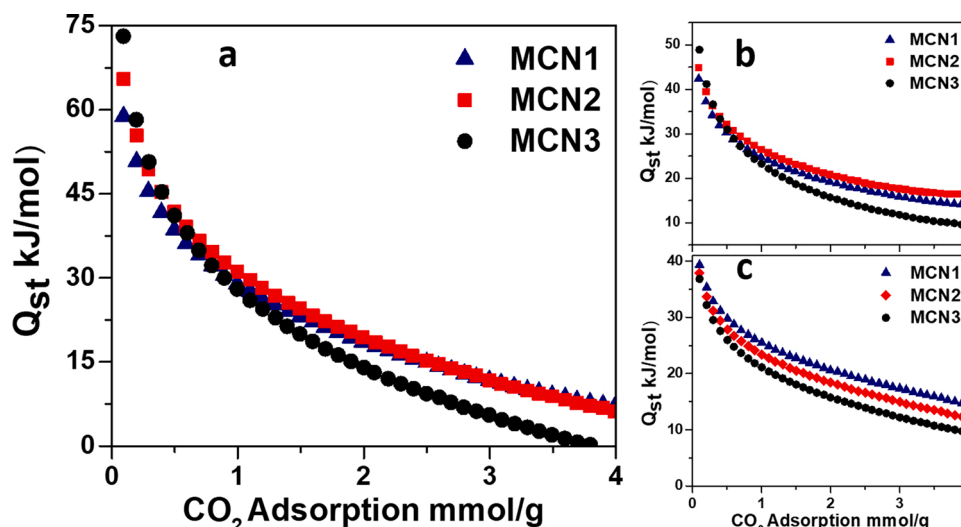


Fig. 4. Comparison of isosteric heat of adsorption (Q_{st}) as a function of CO₂ uptake in (a) 0–250 mbar (b) 250–500 mbar and (c) 500–1000 mbar pressure regimes.

Table 2
CO₂ uptake capacity and isosteric heat of adsorption values of MCN materials.

| Sample | CO ₂ capacity (mmol/g) | | | *Initial isosteric heat of adsorptions Q_{st} ΔH_{ads} kJ/mol | | | Ratio 0–250/500–1000 | Reference |
|----------------------|-----------------------------------|-------|-------|---|--------------|---------------|----------------------|-----------|
| | 0 °C | 25 °C | 75 °C | 0–250 mbar | 250–500 mbar | 500–1000 mbar | | |
| MCN1 | | 2.43 | 1.38 | 58 | 43 | 39 | 1.48 | This work |
| MCN2 | | 2.48 | 1.60 | 67 | 45 | 38 | 1.78 | This work |
| MCN3 | | 2.53 | 1.74 | 73 | 49 | 37 | 2.02 | This work |
| AC | | 2.40 | 0.76 | | | | | This work |
| X13 | | 3.90 | – | | | | | [13] |
| Porous Carbon | 7.60 | 2.49 | – | | | | | [46] |
| NaNH ₂ -C | 5.58 | 3.41 | – | | | | | [39] |
| PEHA@CNS | | 2.65 | 5.45 | | | | | [38] |
| Cu-BTC | | 4.7 | 0.63 | | | | | [49] |

materials, we calculated the isosteric heat of adsorptions (Q_{st}) values using isotherm data collected at different temperatures [13,43,48]. The results show that at low pressure, MCN3 has a significantly higher initial Q_{st} ~73 kJ/mol, values typically seen for the presence of terminal and secondary amines. (Fig. 4a). The MCN1 has the lowest Q_{st} ~58 kJ/mol which can be attributed to a relatively less number of free NH₂ sites in the materials (Fig. 4b). At higher CO₂ pressure (> 250 mbar), a small difference in Q_{st} values for MCN1 indicates similar nature of binding sites and coverage of the majority of available sites. To explain this further, we calculated the initial isosteric heat of adsorption values in different pressure regimes (Table 2). The results reveal the differences in types and concentration of CO₂ adsorption sites in MCN materials. The high Q_{st} values in the 0–250 mbar regime suggest high affinity binding sites (e.g. terminal amines) are prominent in this region, which follows an order MCN3 > MCN2 > MCN1 in terms of their abundance. Notably, thermal condensation of amine precursors may likely result in formation of a variety of amines (terminal amine, piperidine, aniline, pyridine, triazine, and carbon ring, etc.) having differences in CO₂ affinity thereby influencing the material uptake behavior [35,47]. In particular, thermal condensation of triethylenetetramine in MCN3 generates structure with less conjugation having more terminal amine sites in comparison to the other materials (FTIR, XPS results), thus show high uptake in low pressure regime.

Beyond 500 mbar high initial heat of adsorption of MCN1 also infers that it is the type of amines that influence the uptake behavior, as the XPS results show types of C and N present in MCN3 differ from MCN1 and MCN2. Furthermore, the (0–250)/(500–1000) ratio of heats of adsorption shows that this trend did not just reflect the number of CO₂ adsorption sites, but rather a relative increase in the number of high affinity binding sites for materials with higher nitrogen content. This is

significant as it provides the basis for how to design an adsorbent with a desired Q_{st} by tuning structures with a particular type and number of N sites in the material. It is noted that Q_{st} values throughout the adsorption process are still lower than the chemical bonding enthalpy of the nitrogen lone pair with CO₂ ~80 kJ/mol in liquid amine solutions. This data suggests that nitrogen-rich carbon structures reported here have moderately high chemisorption strength due to N embedded surfaces, which can be tuned to achieve easy-on/easy-off sorbent for CO₂ capture at application specific temperature.

3.1. Conclusions

In summary, the nitrogen content of mesoporous carbon nitrides can easily be enhanced and such modification has a direct effect on CO₂ uptake capacity at low pressure and higher temperature. It is demonstrated that the isosteric heat of adsorption, which is a function of nitrogen type and content, can be tuned to design the binding energetics of the material. Further, MCN materials have the potential for their use as CO₂ sorbent or membranes. The work highlight the role of structural transformations needed to control the type and environment of CO₂ binding sites in designing new sorbent materials.

Declaration of Competing Interest

The authors report no declarations of interest.

Appendix A. Supplementary data

Supplementary material related to this article can be found, in the online version, at doi:<https://doi.org/10.1016/j.jcou.2020.101375>.

References

- [1] A.M. Cormos, C. Dinca, L. Petrescu, D. Andreea Chisalita, S. Szima, C.C. Cormos, Carbon capture and utilisation technologies applied to energy conversion systems and other energy-intensive industrial applications, *Fuel* 211 (2018) 883–890, <https://doi.org/10.1016/j.fuel.2017.09.104>.
- [2] R.M. Cuéllar-Franca, A. Azapagic, Carbon capture, storage and utilisation technologies: a critical analysis and comparison of their life cycle environmental impacts, *J. CO₂ Util.* 9 (2015) 82–102, <https://doi.org/10.1016/j.jcou.2014.12.001>.
- [3] T. N. Borhani, M. Wang, Role of solvents in CO₂ capture processes: the review of selection and design methods, *Renewable Sustainable Energy Rev.* 114 (2019) 109299, <https://doi.org/10.1016/j.rser.2019.109299>.
- [4] S. Zeng, X. Zhang, L. Bai, X. Zhang, H. Wang, J. Wang, D. Bao, M. Li, X. Liu, S. Zhang, Ionic-liquid-based CO₂ capture systems: structure, interaction and process, *Chem. Rev.* 117 (2017) 9625–9673, <https://doi.org/10.1021/acs.chemrev.7b00072>.
- [5] J. Yu, L.H. Xie, J.R. Li, Y. Ma, J.M. Seminario, P.B. Balbuena, CO₂ capture and separations using MOFs: computational and experimental studies, *Chem. Rev.* 117 (2017) 9674–9754, <https://doi.org/10.1021/acs.chemrev.6b00626>.
- [6] D.J. Heldebrant, P.K. Koech, V.A. Glezakou, R. Rousseau, D. Malhotra, D.C. Cantu, Water-lean solvents for post-combustion CO₂ capture: fundamentals, uncertainties, opportunities, and outlook, *Chem. Rev.* 117 (2017) 9594–9624, <https://doi.org/10.1021/acs.chemrev.6b00768>.
- [7] G.T. Rochelle, Amine scrubbing for CO₂ capture, *Science* (80-) 325 (2009) 1652–1654, <https://doi.org/10.1126/science.1176731>.
- [8] Q. Wang, J. Luo, Z. Zhong, A. Borgna, CO₂ capture by solid adsorbents and their applications: current status and new trends, *Energy Environ. Sci.* 4 (2011) 42–55, <https://doi.org/10.1039/c0ee00064g>.
- [9] E.B. Rinker, S.S. Ashour, Orville C. Sandall, Absorption of Carbon Dioxide in aqueous blends of Diethanolamine and methylethanolamine, *Ind. Eng. Chem.* 39 (2000) 4346–4356, http://rochelle.che.utexas.edu/files/2015/02/Chakravarti_Thesis_1992.pdf.
- [10] B. Arstad, R. Blom, O. Swang, CO₂ absorption in aqueous solutions of alkanolamines: mechanistic insight from quantum chemical calculations, *J. Phys. Chem. A* 111 (2007) 1222–1228, <https://doi.org/10.1021/jp065301v>.
- [11] M. Gupta, H.F. Svendsen, Understanding carbamate formation reaction thermochemistry of amino acids as solvents for postcombustion CO₂ capture, *J. Phys. Chem. B* 123 (2019) 8433–8447, <https://doi.org/10.1021/acs.jpcc.9b06447>.
- [12] B. Wang, A.P. Côté, H. Furukawa, M. O’Keeffe, O.M. Yaghi, Colossal cages in zeolitic imidazolate frameworks as selective carbon dioxide reservoirs, *Nature* 453 (2008) 207–211, <https://doi.org/10.1038/nature06900>.
- [13] H. Yang, A.M. Khan, Y. Yuan, S.C. Tsang, Mesoporous silicon nitride for reversible CO₂ capture, *Chem. Asian J.* 7 (2012) 498–502, <https://doi.org/10.1002/asia.201100615>.
- [14] F.J. Uribe-romo, C.B. Knobler, M.O. Keffe, O.M. Yaghi, Capture properties of zeolitic imidazolate frameworks, *Acc. Chem. Res.* 43 (2010) 58–67, <http://www.ncbi.nlm.nih.gov/pubmed/19877580>.
- [15] A. Modak, A. Bhaumik, Porous carbon derived via KOH activation of a hypercrosslinked porous organic polymer for efficient CO₂, CH₄, H₂ adsorptions and high CO₂/N₂ selectivity, *J. Solid State Chem.* 232 (2015) 157–162, <https://doi.org/10.1016/j.jssc.2015.09.022>.
- [16] H. Liu, Y. Zhang, R. Li, X. Sun, S. Désilets, H. Abou-Rachid, M. Jaidann, L.S. Lussier, Structural and morphological control of aligned nitrogen-doped carbon nanotubes, *Carbon* 48 (2010) 1498–1507, <https://doi.org/10.1016/j.carbon.2009.12.045>.
- [17] G. Singh, K.S. Lakhi, S. Sil, S.V. Bhosale, I.Y. Kim, K. Albahily, A. Vinu, Biomass derived porous carbon for CO₂ capture, *Carbon* 148 (2019) 164–186, <https://doi.org/10.1016/j.carbon.2019.03.050>.
- [18] A. Zukal, J. Pawlesa, J. Čejka, Isothermic heats of adsorption of carbon dioxide on zeolite MCM-22 modified by alkali metal cations, *Adsorption* 15 (2009) 264–270, <https://doi.org/10.1007/s10450-009-9178-5>.
- [19] A. Pulido, P. Nachtigall, A. Zukal, I. Dominguez, J. Čejka, Adsorption of CO₂ on sodium-exchanged ferrierites: the bridged CO₂ complexes formed between two extraframework cations, *J. Phys. Chem. C* 113 (2009) 2928–2935, <https://doi.org/10.1021/jp810038b>.
- [20] A. Demessence, D.M.D. Alessandro, M.L. Foo, J.R. Long, Strong CO₂ binding in a water-stable, triazolate-bridged metal-organic framework functionalized with ethylenediamine, *J. Am. Chem. Soc.* 131 (2009) 8784–8786, <https://doi.org/10.1021/ja903411w>.
- [21] J. De-en, M.M. Shannon, D. Sheng (Eds.), *Materials for Carbon Capture*, First, Wiley-VCH Verlag GmbH & Co. KGaA, 2019.
- [22] L. Rao, R. Ma, S. Liu, L. Wang, Z. Wu, J. Yang, X. Hu, Nitrogen enriched porous carbons from D-glucose with excellent CO₂ capture performance, *Chem. Eng. J.* 362 (2019) 794–801, <https://doi.org/10.1016/j.cej.2019.01.093>.
- [23] N. Hiyoshi, K. Yogo, T. Yashima, Adsorption characteristics of carbon dioxide on organically functionalized SBA-15, *Microporous Mesoporous Mater.* 84 (2005) 357–365, <https://doi.org/10.1016/j.micromeso.2005.06.010>.
- [24] C. Kno, V. Hornebecq, P.L. Llewellyn, Study of carbon dioxide adsorption on mesoporous aminopropylsilane-functionalized silica and titania combining microcalorimetry and in situ infrared spectroscopy, *J. Phys. Chem. C* 113 (2009) 21726–21734.
- [25] Y. Belmabkhout, G. De Weireld, A. Sayari, Amine-bearing mesoporous silica for CO₂ and H₂S removal from natural gas and biogas, *Langmuir* 25 (2009) 13275–13278, <https://doi.org/10.1021/la903238y>.
- [26] B. Arstad, H. Fjellvåg, K.O. Kongshaug, O. Swang, R. Blom, Amine functionalised metal organic frameworks (MOFs) as adsorbents for carbon dioxide, *Adsorption* 14 (2008) 755–762, <https://doi.org/10.1007/s10450-008-9137-6>.
- [27] M. Nandi, K. Okada, A. Dutta, A. Bhaumik, J. Maruyama, D. Derks, H. Uyama, Unprecedented CO₂ uptake over highly porous N-doped activated carbon monoliths prepared by physical activation, *Chem. Commun.* 48 (2012) 10283–10285, <https://doi.org/10.1039/c2cc35334b>.
- [28] D. Mantzalis, N. Asproulis, D. Drikakis, Enhanced carbon dioxide adsorption through carbon nanoscrolls, *Phys. Rev. E - Stat. Nonlinear, Soft Matter Phys.* 84 (2011), 066304, <https://doi.org/10.1103/PhysRevE.84.066304>.
- [29] S.C. Qi, J.K. Wu, J. Lu, G.X. Yu, R.R. Zhu, Y. Liu, X.Q. Liu, L.B. Sun, Underlying mechanism of CO₂ adsorption onto conjugated azacyclo-copolymers: N-doped adsorbents capture CO₂ chiefly through acid-base interaction? *J. Mater. Chem. A Mater. Energy Sustain.* 7 (2019) 17842–17853, <https://doi.org/10.1039/c9ta04785a>.
- [30] K. Li, J.D. Kress, D.S. Mebane, The mechanism of CO₂ adsorption under dry and humid conditions in mesoporous silica-supported amine sorbents, *J. Phys. Chem. C* 120 (2016) 23683–23691, <https://doi.org/10.1021/acs.jpcc.6b08808>.
- [31] A. Demessence, D.M. D’Alessandro, M.L. Foo, J.R. Long, Strong CO₂ binding in a water-stable, triazolate-bridged metal-organic framework functionalized with ethylenediamine, *J. Am. Chem. Soc.* 131 (2009) 8784–8786, <https://doi.org/10.1021/ja903411w>.
- [32] R. Vaidhyanathan, S.S. Iremonger, K.W. Dawson, G.K.H. Shimizu, An amine-functionalized metal organic framework for preferential CO₂ adsorption at low pressures, *Chem. Commun.* (2009) 5230–5232, <https://doi.org/10.1039/b911481e>.
- [33] M.D. Soutullo, C.I. Odom, B.F. Wicker, C.N. Henderson, A.C. Stenson, J.H. Davis, Reversible CO₂ capture by unexpected plastic-, resin-, and gel-like ionic soft materials discovered during the combi-click generation of a TSIL library, *Chem. Mater.* 19 (2007) 3581–3583, <https://doi.org/10.1021/cm0705690>.
- [34] X. Ma, X. Wang, C. Song, “Molecular basket” sorbents for separation of CO₂ and H₂S from various gas streams, *J. Am. Chem. Soc.* 131 (2009) 5777–5783, <https://doi.org/10.1021/ja8074105>.
- [35] W. Lu, J.P. Sculley, D. Yuan, R. Krishna, Z. Wei, H.C. Zhou, Polyamine-tethered porous polymer networks for carbon dioxide capture from flue gas, *Angew. Chemie - Int. Ed.* 51 (2012) 7480–7484, <https://doi.org/10.1002/anie.201202176>.
- [36] H.L. Peng, J.B. Zhang, J.Y. Zhang, F.Y. Zhong, P.K. Wu, K. Huang, J.P. Fan, F. Liu, Chitosan-derived mesoporous carbon with ultrahigh pore volume for amine impregnation and highly efficient CO₂ capture, *Chem. Eng. J.* 359 (2019) 1159–1165, <https://doi.org/10.1016/j.cej.2018.11.064>.
- [37] K. Huang, S.H. Chai, R.T. Mayes, G.M. Veith, K.L. Browning, M.A. Sakwa-Novak, M.E. Potter, C.W. Jones, Y.T. Wu, S. Dai, An efficient low-temperature route to nitrogen-doping and activation of mesoporous carbons for CO₂ capture, *Chem. Commun.* 51 (2015) 17261–17264, <https://doi.org/10.1039/c5cc05619e>.
- [38] K. Huang, F. Liu, J.P. Fan, S. Dai, Open and hierarchical carbon framework with ultralarge pore volume for efficient capture of carbon dioxide, *ACS Appl. Mater. Interfaces* 10 (2018) 36961–36968, <https://doi.org/10.1021/acsmi.8b12182>.
- [39] K. Huang, Z.L. Li, J.Y. Zhang, D.J. Tao, F. Liu, S. Dai, Simultaneous activation and N-doping of hydrothermal carbons by NaNH₂: an effective approach to CO₂ adsorbents, *J. CO₂ Util.* 33 (2019) 405–412, <https://doi.org/10.1016/j.jcou.2019.07.012>.
- [40] A. Zukal, I. Dominguez, J. Mayerová, J. Čejka, Functionalization of delaminated zeolite ITQ-6 for the adsorption of carbon dioxide, *Langmuir* 25 (2009) 10314–10321, <https://doi.org/10.1021/la901156z>.
- [41] A. Sayari, Y. Belmabkhout, Stabilization of amine-containing CO₂ adsorbents: dramatic effect of water vapor, *J. Am. Chem. Soc.* 132 (2010) 6312–6314, <https://doi.org/10.1021/ja1013773>.
- [42] A. Vinu, Two-dimensional hexagonally-ordered mesoporous carbon nitrides with tunable pore diameter, surface area and nitrogen content, *Adv. Funct. Mater.* 18 (2008) 816–827, <https://doi.org/10.1002/adfm.200700783>.
- [43] S.N. Talapaneni, S. Anandan, G.P. Mane, C. Anand, D.S. Dhawale, S. Varghese, A. Mano, T. Mori, A. Vinu, Facile synthesis and basic catalytic application of 3D mesoporous carbon nitride with a controllable bimodal distribution, *J. Mater. Chem.* 22 (2012) 9831–9840, <https://doi.org/10.1039/c2jm30229b>.
- [44] X. Liu, S.C. Qi, A.Z. Peng, D.M. Xue, X.Q. Liu, L.B. Sun, Foaming effect of a polymer precursor with a low N content on fabrication of N-Doped porous carbons for CO₂ capture, *Ind. Eng. Chem. Res.* 58 (2019) 11013–11021, <https://doi.org/10.1021/acs.iecr.9b02063>.
- [45] D. Wei, Y. Liu, Y. Wang, H. Zhang, L. Huang, G. Yu, Synthesis of n-doped graphene by chemical vapor deposition and its electrical properties, *Nano Lett.* 9 (2009) 1752–1758, <https://doi.org/10.1021/nl803279t>.
- [46] J.Y. Zhang, J.B. Zhang, M. Li, Z. Wu, S. Dai, K. Huang, Solvent-free and one-pot synthesis of ultramicroporous carbons with ultrahigh nitrogen contents for sulfur dioxide capture, *Chem. Eng. J.* 391 (2020), <https://doi.org/10.1016/j.cej.2019.123579>.
- [47] A. Demessence, D.M. D’Alessandro, M.L. Foo, J.R. Long, Strong CO₂ binding in a water-stable, triazolate-bridged metal-organic framework functionalized with ethylenediamine, *J. Am. Chem. Soc.* 131 (2009) 8784–8786, <https://doi.org/10.1021/ja903411w>.
- [48] S.R. Caskey, A.G. Wong-Foy, A.J. Matzger, Dramatic tuning of carbon dioxide uptake via metal substitution in a coordination polymer with cylindrical pores, *J. Am. Chem. Soc.* 130 (2008) 10870–10871, <https://doi.org/10.1021/ja8036096>.
- [49] Z. Liang, M. Marshall, A.L. Chaffee, CO₂ adsorption-based separation by metal organic framework (Cu-BTC) versus zeolite (13X), *Energy Fuels* 23 (2009) 2785–2789, <https://doi.org/10.1021/ef800938e>.